Journal of Alloys and Compounds 806 (2019) 246–253

Contents lists available at ScienceDirect

Journal of Alloys and Compounds

journal homepage: http://www.elsevier.com/locate/jalcom

Pronounced nanoindentation creep deformation in Cu-doped CoFe-based metallic glasses

C.C. Yuan [a, b, *], Z.W. Lv [a], C.M. Pang [a], W.W. Zhu [a], Xun-Li Wang [b], B.L. Shen [a, **]

[a] School of Materials Science and Engineering, Jiangsu Key Laboratory for Advanced Metallic Materials, Southeast University, Nanjing, 211189, China
[b] Department of Physics, City University of Hong Kong, Kowloon, Hong Kong, China

ARTICLE INFO

Article history:
Received 13 April 2019
Received in revised form
25 June 2019
Accepted 19 July 2019
Available online 19 July 2019

Keywords:
Deformation
Plasticity and creep
Disordered structures
Metallic glasses

ABSTRACT

By using nanoindentation techniques combined with atomic force microscopy, a pronounced creep behavior at ambient temperature as demonstrated by small creeping stress exponents was observed in $(Co_{0.7}Fe_{0.3})_{0.68}B_{0.219}Si_{0.051}Nb_{0.05}$ metallic glass with 0.5 at.% Cu addition. Such obvious creep deformation is due to the precipitation of Co(Fe)-rich clusters induced by the chemical effect of Cu. It promotes the formation of the weakly bonded structure and thereby the generation of plenty of excess free volume during the nucleation and propagation of multiple shear bands in the process of deformation, which contributes to a steady creep behavior and large plasticity. Our work provides a microscopic understanding of creep behaviors in Cu-doped metallic glasses, which might also guide for improving the plasticity of these alloys.

1. Introduction

Nanoindentation is frequently used to study the mechanical responding during creep, serrated flow, phase transformation, etc., for structural materials such as ceramics, metals, and glasses [1,2]. Indentation creep arising from the motion/diffusion of atoms or defects under the loading condition is often conducted to describe time-dependent plastic deformations of the material [3]. It always happens accompanied by the competition of the structural relaxation and the anelastic strain recovery [4,5]. Such evolution of structure during deformation always involves redistributions of free volume and rearrangements of atomic species [6,7]. For Zr- [8,9], U- [10], TiZrHfBeCu(Ni)- [11], especially Fe-based [12,13] metallic glasses (MGs) with glass transition temperature (T_g) much higher than the room temperature, the localized nanoindentation creep at room temperature (~0.35–0.45 T_g) is highly relying on the propagation rate of free volume during the deformation [13]. Thus, the studies on the creep behavior of these MGs may help us better understand the underlying mechanism of their instantaneous plasticity [2,3,13].

It has been reported that the soft magnetic properties [14,15] and the mechanical performance of ferromagnetic MGs [16–19] can be enhanced significantly as the addition of Cu element. It often leads to the nucleation of α-(Co, Fe) grains in Co/Fe-based MGs [17,20,21]. Some works point out such nanoscale α-(Co, Fe) nuclei [16,17,19] can boost the initiation of multiple shear bands and lead to the large plasticity of MGs [22]. However, the convincing experimental evidence for such plasticity deformation process is still missing, especially the mechanical responses at the microscopic scale.

In this work, by using nanoindentation techniques, the creep behavior of $(Co_{0.7}Fe_{0.3})_{0.68}B_{0.219}Si_{0.051}Nb_{0.05}$ at ambient temperature with a small amount of Cu doping was investigated in details. We found that the addition of Cu promotes the creation of free volume during creep deformations, which effectively enhances the indentation creep of the material, along with the reduction of the loading-rate sensitivity. The excess free volume generated continuously during deformation leads to lower creeping stress exponents in this amorphous alloy system, which is quite different from the defect nucleation mechanism that reported in crystalline alloys [23,24]. It stimulates the nucleation of a large number of "flow defects", thereby the formation of multiple shear bands. This might explain the improvement of plasticity in many Cu-doped MGs [16–19].

* Corresponding author. School of Materials Science and Engineering, Jiangsu Key Laboratory for Advanced Metallic Materials, Southeast University, Nanjing, 211189, China.
** Corresponding author.
E-mail addresses: yuanchenchenneu@hotmail.com (C.C. Yuan), blshen@seu.edu.com (B.L. Shen).

https://doi.org/10.1016/j.jallcom.2019.07.226
0925-8388/

2. Experimental

Alloy ingots with nominal compositions of $[(Co_{0.7}Fe_{0.3})_{0.68}B_{0.219}Si_{0.051}Nb_{0.05}]_{100-x}Cu_x$ (x = 0, 0.5) (denoted as Cu0 and Cu0.5) were prepared by arc melting mixtures of pure Co (99.99 at.%), Fe (99.99 at.%), B (99.999 at.%), Si (99.99 at.%), Nb (99.95 at.%), Cu (99.995 at.%) in a high-purity argon atmosphere. The thermal stability and the associated thermodynamic parameters of glassy samples were examined by NETZSCH 404 F3 differential scanning calorimeter (DSC) at a heating rate of 40 $K \cdot min^{-1}$.

The nanoindentation tests were conducted using a NanoTest Vantage (Micro Materials Ltd) with a standard Berkovich diamond indenter. The cylindrical rods for nanoindentation experiments with a diameter of 1 mm were fabricated by a copper mold casting method. The specimens, cut from cylindrical amorphous rods, were mechanically polished mirrorlike on one side before the nanoindentation testing. The load and displacement resolutions of the machine were 3 nN and 0.001 nm, respectively. The machine compliance calibration for the transducer-tip configuration and tip area functional calibration was performed with a standard fused silica sample before proceeding with all indentation experiments. Experiments at constant loading rates of 0.1, 0.5, 1, 5, 10, 50, and 100 mN/s were carried out to a load limit of 50 mN followed by a holding period of 100 s and then unloaded at the same loading rate. At least five indentation tests were carried out under each condition to minimize the influence of noises and discard those results biased significantly against the others. Thermal drift is a negligible constant during the entire indentation creep experiment at the given time. The surface morphology around the indents was recorded by Veeco Dimension ICON atomic force microscope (AFM).

3. Results and discussion

Fig. 1 (a) and (b) present load-displacement (*P-h*) curves of Cu0

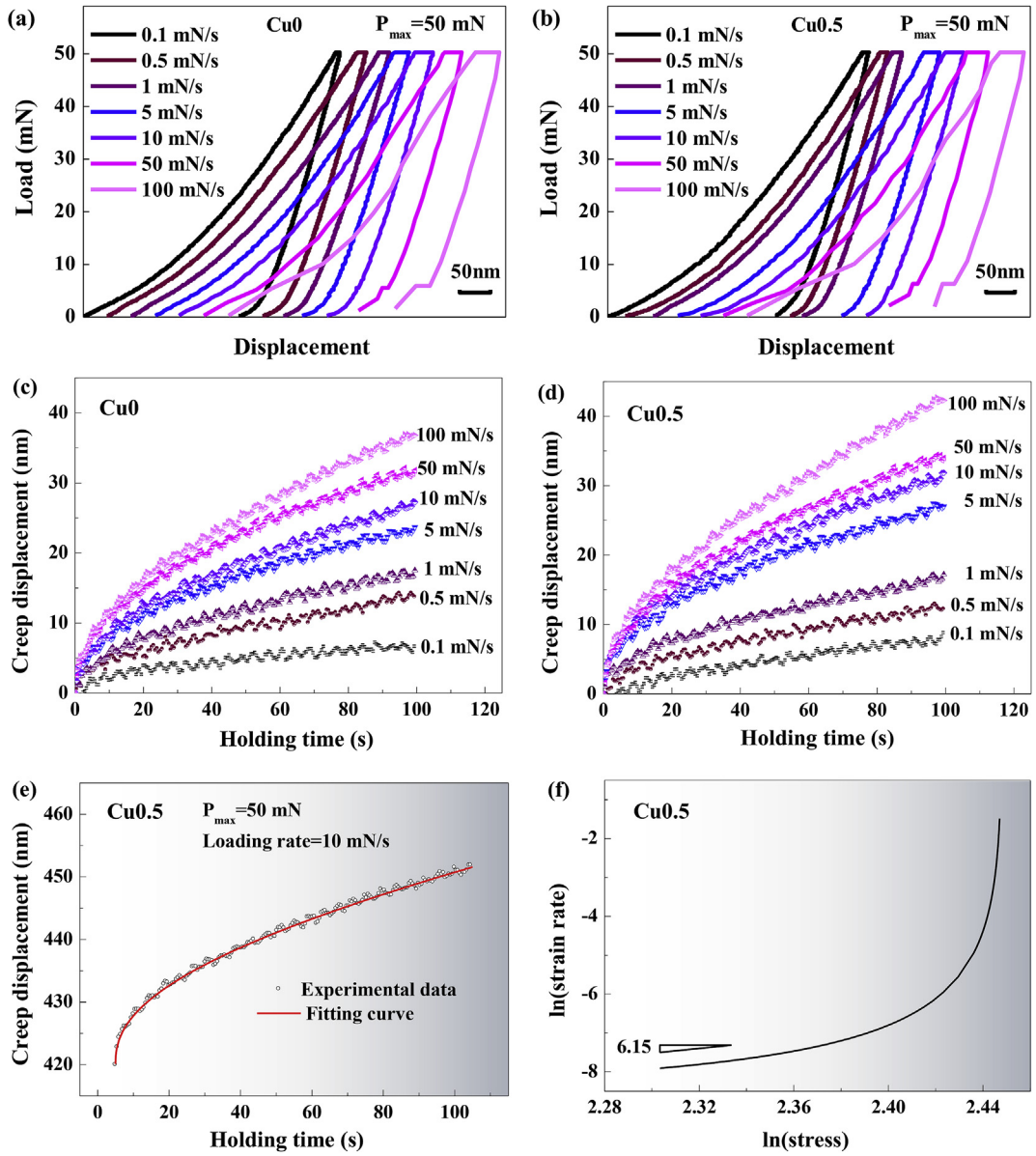

Fig. 1. Creep deformation of the as-cast Cu0 and Cu0.5 MG samples. Typical load - displacement (P - h) curves under different loading rates of Cu0 (a) and Cu0.5 (b) MGs. The curves in (a) and (b) offset from the origin for clear viewing. The creep displacement during load holding period under different rates of Cu0 (a) and Cu0.5 (b) MGs. (e) Experimental and fitted creep curves of Cu0.5 at a loading rate of 10 mN/s; (f) the corresponding ln (strain rate) - ln (stress) plot.

and Cu0.5 MG samples during nanoindentation under loading rates ranging from 0.1 to 100 mN/s at a load limit of 50 mN, where P is loading force and h the instantaneous indenter displacement. The recorded creep displacement curves during the constant load holding are shown in Fig. 1 (c) and (d). It can be seen that during the load holding period, the indenter displacement initially increases sharply with time. After followed by a decreasing strain rate, it exhibits a relative steady-state behavior, i.e., the strain almost increases linearly with time. This is consistent with the observations in other MGs such as $Pd_{40}Cu_{30}Ni_{10}P_{20}$ [25], $Cu_{50}Zr_{50}$ [8], $Fe_{41}Co_7Cr_{15}Mo_{14}C_{15}B_6Y_2$ [12], and $\{[(Fe_{0.6}Co_{0.4})_{0.75}B_{0.2}Si_{0.05}]_{0.96}Nb_{0.04}\}_{96}Cr_4$ [13] MGs during nanoindentations at room temperature, as well as in some crystalline materials. Nanoindentation creeps of Ce- and La-based MGs with low T_g [26,27] carried out at room temperature (~0.75 T_g) display a similar deformation behavior, their time-dependent displacement curves obey a generalized Kelvin model [27]. Moreover, we find that in Fig. 1 (c) and (d), the magnitude of creep deformation of two Co(Fe)-based MGs increases rapidly with increasing the loading rate, suggesting a strong loading rate sensitivity, which has also been observed in many other MGs [8,12,13,25–27]. Compared with Cu0 MG, the composition with 0.5 at.% Cu doping exhibits a less creep resistance at the same loading rate.

Fig. 1 (e) shows the typical displacement-time (h-t) curve of Cu0.5 MG with a loading rate of 10 mN/s during the load holding period at the maximum loading of 50 mN, where t is the indentation time. It can be fitted using the empirical equation [28]:

$$h\,(t) = h_0 + a(t - t_0)^b + kt \tag{1}$$

where t_0, h_0, a, b, and k are fitting constants. Thereinto, t_0 is the start time of creep processes and h_0 the initial position of the indenter. Accordingly, the strain rate $\dot{\varepsilon}$ can be derived by h with the depth-sensing indentation technique [29]:

$$\dot{\varepsilon} = \dot{h}/h = \frac{1}{h}\frac{dh}{dt} \tag{2}$$

As shown in Fig. 1 (e), the displacement-time curve can be fitted well with Eq. (1), which gives rise to the creep strain rate $\dot{\varepsilon}$ by taking Eq. (2). The mean stress σ can be derived by Ref. [12]:

$$\sigma = P/24.5h^2 \tag{3}$$

Where P is the applied load on the sample. The corresponding $\ln\dot{\varepsilon}$ versus $\ln\sigma$ is plotted in Fig. 1(f). At the first stage of the load holding period, the sample shows a transient creep behavior, where the penetration deepens at a very high strain rate. When the steady state is achieved, the strain rate gradually saturates and almost keeps constant at the order of about 10^{-4}. During the steady creep deformation, the relationship between the strain rate $\dot{\varepsilon}$ and the characteristic stress σ can be described by an empirical power-law equation [30,31]:

$$\dot{\varepsilon} = k\sigma^n \tag{4}$$

where the pre-factor k is a temperature dependence constant, the stress exponent n as an indicator of time-dependent deformation mechanism can be calculated by the slope of the ln-ln plot of $\dot{\varepsilon}$ versus σ under isothermal conditions, i.e., $\partial\ln\dot{\varepsilon}/\partial\ln\sigma$. As seen in Fig. 1(f), the slope becomes constant towards the end of the holding period, exhibiting a steady-state creep behavior with the stress exponent n of 6.15 for the power-law creep.

The derived stress exponent as a function of the indentation loading rate is displayed in Fig. 2. With increasing the loading rate from 0.1 to 100 mN/s, the estimated stress exponent decreases gradually from 29 to 3,19 to 3 for Cu0 and Cu0.5 MGs, respectively,

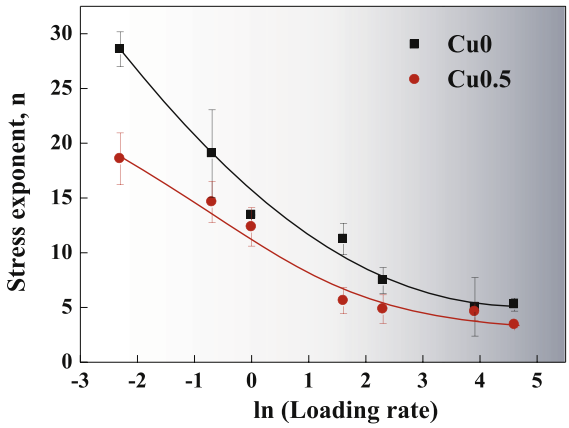

Fig. 2. Steady-state stress exponent, n, of Cu0 and Cu0.5 MGs as a function of indentation loading rates. The solid lines are guides for the eyes.

indicating the high loading-rate sensitivity upon the ascending load rate. The trend of the stress exponent varying with the loading rate in the present study is in agreement with the work of Huang and Xu et al. [12,13]. The values of stress exponent for $\{[(Fe_{0.6}Co_{0.4})_{0.75}B_{0.2}Si_{0.05}]_{0.96}Nb_{0.04}\}_{96}Cr_4$ MG shown by Fu are 28.1 to 4.9 with the loading rate in the range from 1 to 50 mN/s. Apparently, the stress exponents of Cu0 MG are more sensitive to the loading rate. We also find that the value of stress exponents decreases upon Cu doping. It demonstrates that it is easier for Cu-doped MG to creep deformation than for non-Cu MG under the same conditions.

Plastic deformation of MGs normally occurs by shearing clusters of localized atoms, i.e. shear transformation zone (STZ) [32]. Such flow defects in MGs are often described according to the free volume model as density fluctuations with the volume greater than critical value v^*, where v^* is the critical volume of an atom under the frame of a hard-sphere model. When under uniaxial loading, small regions of volume undergo a strain ε_0, the strain rate $\dot{\varepsilon}_u$ can be described as [32,33]:

$$\dot{\varepsilon}_u = \mathrm{A}\,\Delta f exp(-\frac{\gamma v^*}{v_f}) \tag{5}$$

$$\mathrm{A} = 2\nu\frac{\varepsilon_0\nu_0}{\Omega}\,sinh(\frac{\sigma\varepsilon_0\nu_0}{2kT})exp(-\frac{\Delta G^m}{kT}) \tag{6}$$

where γ is a geometrical factor between 0.5 and 1, v_f the free volume, ν the frequency of atomic vibration ($\approx$Debye frequency), Ω the atomic volume (~1.25 v^* [34], 13.2 Å^3 in $Pd_{41}Ni_{10}Cu_{29}P_{20}$ [32]), σ the uniaxial stress, k Boltzmann's constant, T the temperature and ΔG^m the activation energy of atomic motion. The product $\varepsilon_0\nu_0$ is the activation volume of the process, which is about 100–130 Å^3 in MGs [32,35]. For the case of nanoindentation tests, the deformation is supposed to be homogeneous, $\Delta f = 1$. The sample under the indenter always withstands a multiaxial stresses. The relationship between the indentation strain rate $\dot{\varepsilon}$ and the effective strain rate $\dot{\varepsilon}_u$ under the uniaxial stress σ is complex. There is no simple correlation valid for all materials and indenter tips is available [36–39]. Here, we use a simple relation determined by Poisl et al. [38] performed on amorphous selenium based on nanoindentation experiments by using Berkovich diamond indenter:

$$\dot{\varepsilon}_u = C\dot{\varepsilon} \tag{7}$$

where the constant $C = 0.09$ measured under the loading rates of

0.1–10 mN/s with the maximum loading of 10 mN. It has been reported that the value of $C = 0.09$ works well in the Fe(Co)-based bulk MG system such as $\{[(Fe_{0.6}Co_{0.4})_{0.75}B_{0.2}Si_{0.05}]_{0.96}Nb_{0.04}\}_{96}Cr_4$ [13], even though the elastic modulus and hardness of amorphous selenium are 10 and 10–40 GPa, respectively, about 10–20 times lower than that of the Fe(Co)-based MGs [13,40]. According to Eqs. (5)–(7), the indentation strain rate can be simplified as:

$$\dot{\varepsilon} = 11A\, exp(-\frac{\gamma v^*}{v_f}) \tag{8}$$

Since the temperature ascending is not pronounced during nanoindentation processes [41] and the change in σ is small during the load holding period, A can be considered as a constant. Thus, the concentration of free volume as described in Eq. (8) is positively related to the magnitude of strain rates. It means a large amount of free volume could be generated during the deformation process. According to the work of Spaepen et al. [33], under a diffusion-driven model, the amount of free volume created per second $\Delta^+ v_f$ during loading can be given by:

$$\Delta^+ v_f = \frac{\gamma v^*}{v_f}\frac{2kT}{S}[cosh(\frac{\sigma\varepsilon_0\nu_0}{2kT}) - 1]N\nu exp(-\frac{\Delta G^m}{kT})exp(-\frac{\gamma v^*}{v_f}) \tag{9}$$

where N is the total number of atoms and S the material constant. $S = \frac{2}{3}G\frac{1+\mu}{1-\mu}$ [33], where the shear modulus $G \sim 70$–80 GPa for the present studied systems and Poisson's ratio μ is around 0.31 for Fe(Co)-based MGs [34,42]. It gives rise to a constant value of ~95–100 for S. Combining Eq. (8) with Eq. (9), we get:

$$\Delta^+ v_f = 0.09B\dot{\varepsilon} \tag{10}$$

where $B = \frac{NkT}{S}\frac{\gamma v^*}{v_f}\frac{\Omega}{\varepsilon_0 v_0}$, the hyperbolic functions approximate to exponentials at high stress state. Therefore, according to Eq. (10), we can estimate the amount of free volume $\Delta^+ v_f$ per mole produced at different indentation strain rates under the indenter. Here, the total number of atoms N is proposed as Avogadro's constant, 6.022×10^{23} mol^{-1}, T ~298 K, $\gamma v^* \approx 0.5\ \Omega \sim 6.6$ Å^3 [35] ($\gamma \approx 0.6$, v^*~10.56 Å^3), $v_f = \alpha\gamma v^*$ [34], $\alpha \sim 2.2$–2.4% (2.4% is critical value for the plastic instability). Then, B is of about 120 at room temperature. Since B can be considered as a material constant due to the slight change of v_f during deformation, the production rate of free volume has an approximately linear correlation with $\dot{\varepsilon}$, i.e. $\Delta^+ v_f$ booms up with increasing $\dot{\varepsilon}$.

Fig. 3 presents the calculated $\dot{\varepsilon}$ according to the fits of h-t curves and the production rate of free volume $\Delta^+ v_f$ during creep deformations. It is clear that both the creep strain rate and the generation rate of free volume increase significantly with a rapid climbing up of loading rates. The pronounced creeping behavior corresponding to the reduction of stress exponent at a higher loading rate is attributed to a large amount of free volume generated under loading. As shown in Fig. 3 (c), a large amount of free volume is created during the load holding period. It results in a much more homogeneous creep deformation for the sample with higher strain rates, which well explains the high loading rate sensitivity of creeping stress exponents as shown in Fig. 2. Distinguish from the dislocation nucleation mechanism that dominated in crystalline alloys [23,24], the creep behavior of amorphous alloy systems is analogous to a continuous structure relaxation process [6]. The applied loading around the indent accelerates this relaxation processes. It causes the rearrangement of topological configurations at the atomic scale, which facilitates the generation of free volume. The higher the loading rate is, the more obvious is this process. Thus, a pronounced creep behavior can be observed at a high loading rate. More interestingly, we find in Fig. 3 that the creep

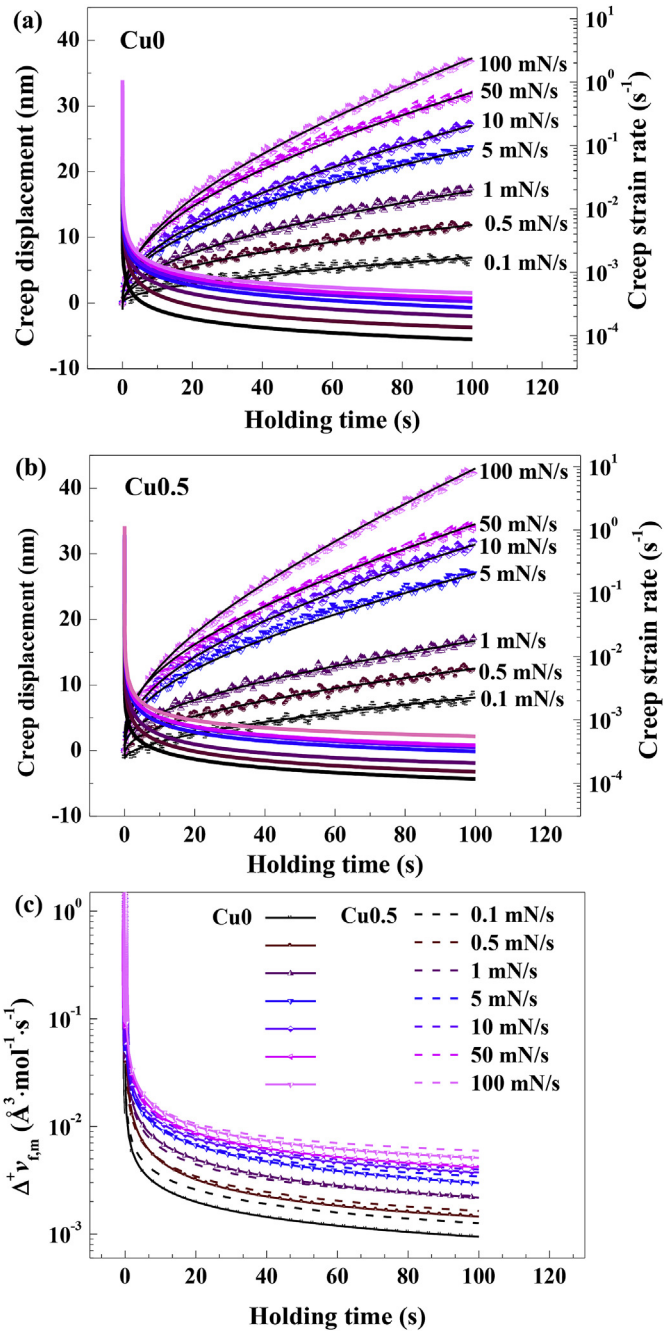

Fig. 3. Experimental creep data, fitting curve, and strain rate of Cu0 (a) and Cu0.5 (b) MGs with loading rate ranging from 0.1 to 100 mN/s. (c) The propagation of free volume as a function of holding time in Cu0 and Cu0.5 MGs.

strain rate as well as the productivity of free volume increases upon alloying with a minor amount of Cu, corresponding to a relatively low stress exponent in Cu0.5 MG. It implies that the reduction of stress exponent with Cu doping is as a result of the high production rate of free volume during creep deformations as well.

According to the work of Slipenyuk et al. [43], the excess free volume (Δv) frozen in glasses can be indirectly measured by DSC according to the following equation:

$$\Delta v \propto \Delta H_{rel} = \int (dQ/dt)dT \tag{11}$$

where ΔH_{rel} is the relaxation enthalpy change on DSC curves. Fig. 4 exhibits the DSC trace of as-cast $[(Co_{0.7}Fe_{0.3})_{0.68}B_{0.219}Si_{0.051}Nb_{0.05}]_{100-x}Cu_x$ (x = 0, 0.5) MGs. The clear glass transition feature and crystallization event(s) of two glasses are characterized in DSC traces at a heating rate of 40 K/min. The parameters such as glass transition temperature T_g, crystallization temperature T_x and $\Delta T_x = (T_x - T_g)$ for these two MGs measured by DSC are 854, 896, and 42 K for the Cu0 system, 850, 892, and 42 K for Cu0.5 system, respectively, which is consistent with the report of ref. 19. It is shown that these parameters are weakly affected by Cu doping. The inset in Fig. 4 presents the magnified view of the thermal traces near T_g, giving the amount of the exothermic heat ΔH_{rel} [44,45]. The slight increase of free volume upon Cu doping indicated by the larger recovery enthalpy ΔH_{rel} during glass transition is found. This phenomenon manifests that a minor addition of Cu stimulates the structural rearrangement into a more unstable and heterogeneous state that possesses more excess free volume.

To further characterize the localized plastic deformation behavior of two MGs, AFM observations around indents are performed, as shown in Fig. 5. A number of partial circular patterned shear bands are observed in the pile-up region around the indent, which reveals that the large plastic deformation occurred during the nanoindentation process [46,47]. Particularly, in Cu0.5 MG, multiple shear bands are observed around the indent, seen in Fig. 5 (c). The significant pile-up around indents indicates the pronounced local deformation occurred during the nanoindentation processes. The pile-up can be evaluated using topographic profiles in Fig. 5 (e) and (f). In the case of Cu0 MG, the pile-up is more obvious around indent locally with a maximum height of 103 nm at the indentation loading rate of 1 mN/s. While in Cu0.5 MG, the pile-up observed around indent only with a maximum height of 28 nm at the indentation loading rate of 1 mN/s. Different from the report of Kim et al. [48], the high pile-up that appears around the indent in Cu0 MG corresponds to a localized deformation and the slight reduction of excess free volume as shown in DSC measurements. While the much lower pile-up of Cu0.5 MG at a wider region around the indent as compared with Cu0 MG indicates a more homogeneous creep deformation behavior upon a minor Cu alloying. Meanwhile, the larger maximum indentation depth, especially at a higher loading rate of more than 10 mN/s, is observed from the topographic profile of Cu0 nanoindentation samples (see Fig. 5 (e)), which increases remarkably with increasing the loading rate from 10 to 100 mN/s. While the MG with 0.5 at.% Cu doping presents a similar maximum indentation depth at different loading rates, exhibiting a more steady mechanical performance under distinct nanoindentation conditions, which is in agreement with the results of stress exponent.

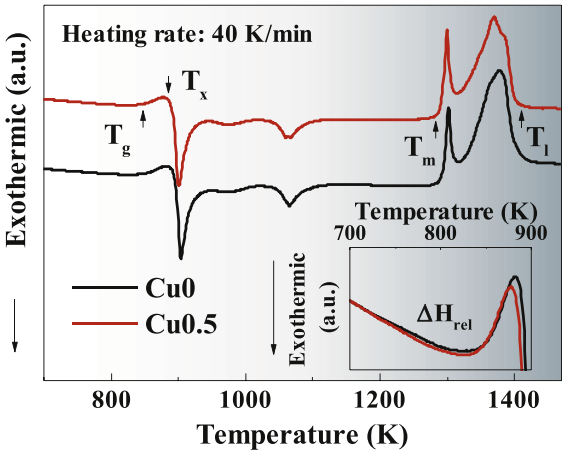

Fig. 4. DSC curve of the as-cast Cu0 and Cu0.5 MG at a heating rate of 40 K/min. The inset shows enthalpy recovery measurements for both samples.

STZs theory [49] proposes that a large amount of evenly distributed free volume leads to a high probability of the nucleation of "flow defects" i.e. STZs and large plasticity. The slightly increased excess free volume that exists in Cu0.5 MG as indicated by DSC may provide some nucleation sites for STZs. More importantly, the excess free volume generated during creep deformations shown in Fig. 3 (c), as manifested by a low creep resistance and the reduced stress exponents, leads to the propagation of plenty of STZs in Cu0.5 MG. The superposition of clusters of localized atoms during shearing when a large number of STZs form, is in favor of a notable creep behavior via homogeneous plastic flows of samples under the indenter as shown in Fig. 5 (f). It explicates the extremely large plasticity of Cu-doped MG [17,19], where the compressive plasticity of 2.5% for the composition with 0.5 at.% Cu alloying was reported [19].

However, when MGs possess an amount of free volume that much larger than that required for the generation and propagation of STZs [32] in an extremely local region, a brittle fracture will happen. A fast motion/diffusion of atoms due to a large amount of free volume locally results in the less resistance of time-dependent deformations. For instance, in the case of Cu0 MG, plenty of free volumes accumulated inside a local region, thereby, leads to worse plasticity via the severe deformation of the sample around the indent as seen in Fig. 5 (e). Such dominant local deformation, corresponding to the large maximum indentation depth and the high pile-up of Cu0 MG observed in nanoindentation measurements (see Fig. 5 (e)), therefore, impedes homogeneous plastic flows of the whole sample. Based on the analyses of indentation behaviors of two MGs and their thermodynamic properties, it is suggested that the free volume that created during deformation rather than the excess free volume that possessed inside the as-cast sample plays a more essential role in determining the plastic deformation behavior of MGs. Plenty of the existing excess free volume trapped inside a local region, instead, deteriorates the plasticity of the material via an inhomogeneous localized deformation. This raises an interesting question that what promotes the generation of free volume in Cu-doped MG during the deformation.

Histograms in Fig. 6 characterize the hardness distribution of two MGs. Each hardness measurement was conducted by using nanoindentation with a loading rate of 1 mN/s at the maximum loading of 50 mN. As seen in Fig. 5, the size of the entire strained zone of an indent is around 5 μm. Although shear bands are developed around the indents, they rarely extend the strain to an outer area as large as the impression itself [50]. Therefore, the distance of 30 μm between two neighboring indents was chosen to avoid the interaction of nearby strained zones. From Fig. 6, we find that the hardness mainly distributes between 12.5 and 14.5 GPa for Cu0 MG, 12.5 and 14.65 GPa for Cu0.5 MG. It shows that the average value of hardness does not change too much with a minor Cu doping. The highest fraction peak value is 12.5% for Cu0 MG when the hardness equals to 13.25 GPa, 12.7% for Cu0.5 MG when hardness equals to 14.25 GPa Cu0.5 MG has two secondary fraction peaks of the same value of 9.52% when the hardness equals to 13.55 and 14.15 GPa, seen in Fig. 6 (b). The superposition of two different normal distributions can be observed in Cu0 MG as well, which causes a relatively low ratio of hardness close to the mean value *H*. It suggests that both non-Cu and Cu-doped MGs have a dual-hardness soft and hard structure at the micron length scale. Compared to Cu0 MG, a wider distribution of hardness for soft phases can be observed in Cu0.5 MG.

The coexistence of soft and hard phases has been widely

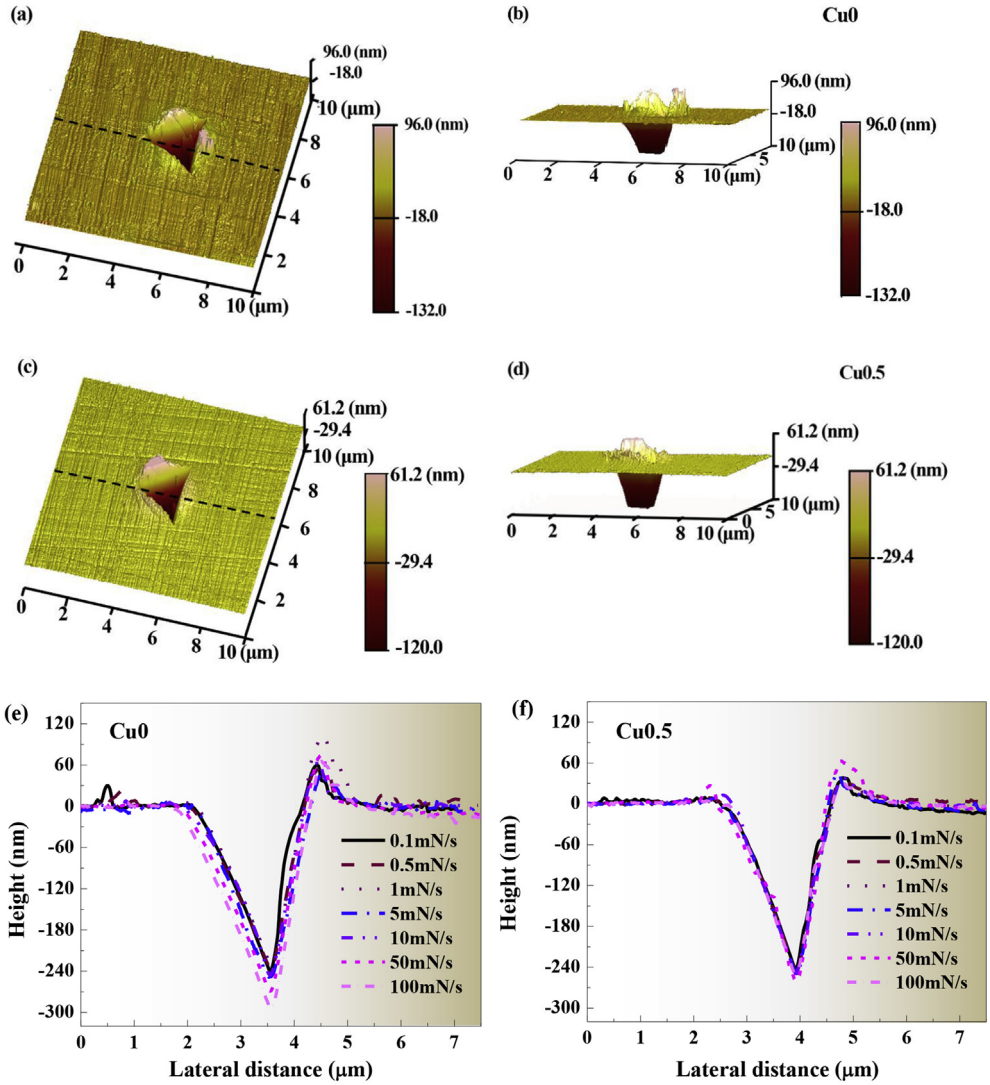

Fig. 5. AFM image of Cu0 under the nanoindentation at a loading rate of 1 mN/s: (a) top view and (b) side view; AFM image of the Cu0.5 under the nanoindentation at a loading rate of 1 mN/s: (c) top view and (d) side view. The cross profile of the indents after nanoindentation for Cu0 (e) and Cu0.5 (f) MG samples.

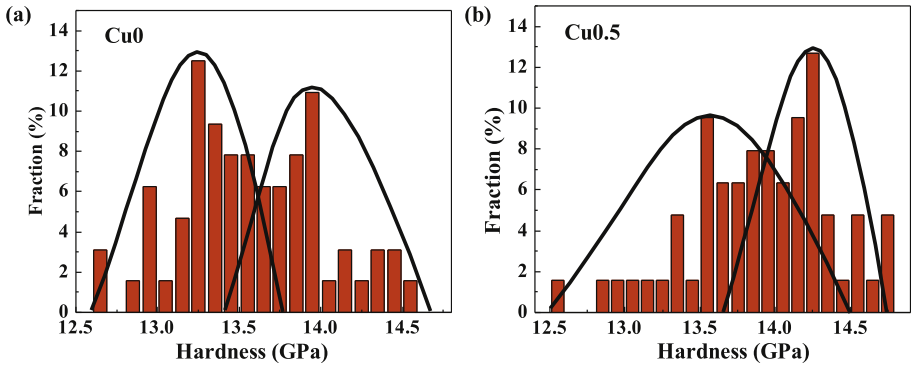

Fig. 6. Hardness of Cu0 (a) and Cu0.5 (b) MGs studied by the nanoindentation.

reported in numerous MGs [51–57]. According to the hardness investigated here, soft regions correspond to weakly bonded regions (yellow regions), while hard regions correspond to strongly bonded regions (blue regions), as seen in Fig. 7. Such coexistence of weakly bonded and strongly bonded regions [58] relates to inhomogeneous properties of the material by introducing the fluctuations of inherent atomic density [59]. As shown in the cross profile of indents in Fig. 5 (e), a localized creep deformation occurs by the accumulation of a large amount of free volume at a restricted region. The productivity of free volume, as well as the

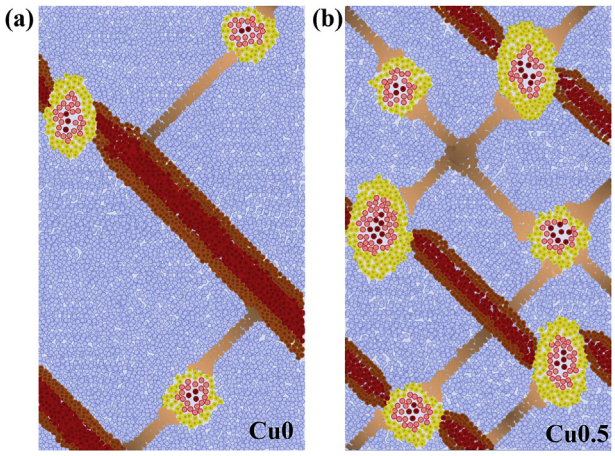

Fig. 7. A schematic diagram for the coexistence of soft (yellow regions) and hard (blue regions) phases and the corresponding plastic behavior in Cu0 (a) and Cu0.5 (b) MGs. (For interpretation of the references to colour in this figure legend, the reader is referred to the Web version of this article.)

homogeneous plastic flow of Cu0 MG, is limited hereby, which causes high resistance to creep deformations with a large stress exponent. Whereas in Cu0.5 MG, a minor addition of Cu benefits weakly bonded regions formed by the precipitation of Co(Fe)-rich clusters/nuclei [15,17,18], which facilitates the energy dissipated during creep deformation processes. It booms the generation of free volume inside weakly bonded regions by a fast motion/diffusion of the active atoms. A high production rate of the free volume can be further provoked when macroscopic defects such as shear bands or microcracks propagate crossing the connected weakly-bonded region as described in Fig. 7 (b). It leads to a pronounced creep behavior by the homogeneous plastic deformation throughout the whole sample under loading.

STZs occur preferentially in weakly bonded regions with low critical shear stress, which would evolve into the nucleation of shear bands once the MG is yieldingly loaded. For Cu0.5 MG, the weakly-bonded region enables multiple shear bands to initiate at different sites simultaneously to accommodate the applied stress, as seen in Figs. 5 (c) and Fig. 7 (b). It prevents a single primary shear band carrying large strain/severe deformation locally that induces a catastrophic fracture. In virtue of the plastic flows of weakly bonded regions, the stress concentration inside shear bands or at the crack tips is mitigated when a shear band or microcrack contacts with the weakly-bonded regions during its propagation process. The retarding and redirection of the initial shear band/microcrack due to the stress concentration then benefits the nucleation of more secondary shear bands/microcracks, accompanied by the propagation of a large amount of free volume, which eventually leads to large macroscopic plasticity. The pronounced creep behavior and superior compressive plasticity [19] of Cu0.5 MG, practically, demonstrate that the distribution of soft/weakly-bonded regions in hard matrix meets the optimum combination conditions in Co(Fe)-based MGs with the composition of 0.5 at.% Cu alloying. Our studies on improving creep behavior of Co(Fe)-based MGs by a minor Cu alloying, thus, can help us understand the plasticity mechanism of these commercial Co(Fe)-based glass composites and may also guide the design of other MGs or glass composites with much larger plasticity.

4. Conclusions

The creep deformation of $[(Co_{0.7}Fe_{0.3})_{0.68}B_{0.219}Si_{0.051}Nb_{0.05}]_{100-x}Cu_x$ (x = 0, 0.5) MGs at ambient temperature was investigated via nanoindentation test. A tiny amount of Cu doping leads to the large creep displacement of Co(Fe)-based MGs. The magnitude of creep displacements increases with increasing the loading rate, exhibiting significant loading-rate sensitivity. This is attributed to the continuous generation of free volume during the creeping process in MGs. A small stress exponent and low pile-up around indents indicate that the plastic flow in Cu-doped MGs is more homogeneous than that in non-Cu MGs. The creep deformation mechanism discussed based on the free volume and STZ theory shows that the generation of free volume during the deformation rather than the excess free volume trapped in a local region plays a more important role in determining the mechanical performance of MGs. We also find that the Cu-doped MG with the large plasticity has a bimodal hardness distribution resulting from the precipitation of nanoscale soft phases in the glassy matrix. Such double-hardness structure effectively improves the plasticity of the MG by the generation of free volume during the initiation of multiple shear bands. A slightly more free volume that created during the load holding period is the reason that leads to a more homogeneous deformation and a smaller stress exponent during the creep deformation of Cu-doped MGs.

Acknowledgments

This work was supported by the National Natural Science Foundation of China (Grant Nos. 51601038 and 51631003), the Natural Science Foundation of Jiangsu Province, China (Grant No. BK20171354), Postdoctoral Fellow under the Hong Kong Scholar Scheme (Grant No. XJ2017048), Jiangsu Key Laboratory for Advanced Metallic Materials (Grant No. BM2007204).

References

[1] A.C. Fischer-Cripps, Nanoindentation, Springer-Verlag, NY, 2002.
[2] C.A. Schuh, T.G. Nieh, A nanoindentation study of serrated flow in bulk metallic glasses, Acta Mater. 51 (1) (2003) 87–99.
[3] A.C. Fischer-Cripps, A simple phenomenological approach to nanoindentation creep, Mater. Sci. Eng. A 385 (1–2) (2004) 74–82.
[4] A. Kursumovic, B. Cantor, Anelastic crossover and creep recovery spectra in $Fe_{40}Ni_{40}B_{20}$ metallic glass, Scr. Mater. 34 (11) (1996) 1655–1660.
[5] K. Csach, Y.A. Filippov, V.A. Khonik, V.A. Kulbaka, V. Ocelik, Nonisothermal strain recovery as a result of irreversible structural relaxation of metallic glasses, Philos. Mag. A 81 (8) (2001) 1901–1915.
[6] A.L. Greer, F. Spaepen, Creep, diffusion, and structural relaxation in metallic glasses, Ann.NY Acad.Sci. 371 (OCT) (1981) 218–237.
[7] A. Vandenbeukel, S. Radelaar, On the kinetics of structural relaxation in metallic glasses, Acta Metall. 31 (3) (1983) 419–427.
[8] B.-G. Yoo, J.-H. Oh, Y.-J. Kim, K.-W. Park, J.-C. Lee, J.-i. Jang, Nanoindentation analysis of time-dependent deformation in as-cast and annealed Cu-Zr bulk metallic glass, Intermetallics 18 (10) (2010) 1898–1901.
[9] Y.H. Chen, J.C. Huang, L. Wang, T.G. Nieh, Effect of residual stresses on nanoindentation creep behavior of Zr-based bulk metallic glasses, Intermetallics 41 (2013) 58–62.
[10] H. Xu, H. Ke, H. Huang, P. Zhang, P. Zhang, T. Liu, Nanoindentation creep behavior of U65Fe30Al5 amorphous alloy, Acta Metall. Sin. 53 (7) (2017) 817–823.
[11] P. Gong, J. Jin, L. Deng, S. Wang, J. Gu, K. Yao, X. Wang, Room temperature nanoindentation creep behavior of TiZrHfBeCu(Ni) high entropy bulk metallic glasses, Mater. Sci. Eng. A-Struct. Mater. Prop. Microstruct. Process. 688 (2017) 174–179.
[12] Y.J. Huang, J. Shen, Y.L. Chiu, J.J.J. Chen, J.F. Sun, Indentation creep of an Fe-based bulk metallic glass, Intermetallics 17 (4) (2009) 190–194.
[13] F. Xu, Z.-l. Long, X.-h. Deng, P. Zhang, Loading rate sensitivity of nanoindentation creep behavior in a Fe-based bulk metallic glass, Trans. Nonferrous Metals Soc. China 23 (6) (2013) 1646–1651.
[14] Z.Z. Li, A. Wang, C.T. Chang, Y.G. Wang, B.S. Dong, FeSiBPNbCu alloys with high glass-forming ability and good soft magnetic properties, Intermetallics 54 (2014) 225–231.
[15] F.L. Kong, H. Men, M.X. Zhang, T.C. Liu, G.Q. Xie, B.L. Shen, Effect of Cu additions on the magnetic properties and microstructure of FeCoNbB nanocrystalline alloy, Appl. Phys. A 108 (1) (2012) 211–215.
[16] B. Shen, H. Men, A. Inoue, Fe-based bulk glassy alloy composite containing in situ formed alpha-(Fe,Co) and (Fe,Co)(23)B-6 microcrystalline grains, Appl. Phys. Lett. 89 (10) (2006) 101915.
[17] X. Li, H. Kato, K. Yubuta, A. Makino, A. Inoue, Effect of Cu on

nanocrystallization and plastic properties of FeSiBPCu bulk metallic glasses, Mater. Sci. Eng. A 527 (10–11) (2010) 2598–2602.
[18] C.L. Zhao, C.C. Dun, Q.K. Man, B.L. Shen, Enhancement of plastic deformation in FeCoNbB bulk metallic glass with super high strength, Intermetallics 32 (2012) 408–412.
[19] G.L. Zhang, Q.Q. Wang, C.C. Yuan, W.M. Yang, J. Zhou, L. Xue, F. Hu, B.A. Sun, B.L. Shen, Effects of Cu additions on mechanical and soft-magnetic properties of CoFeBSiNb bulk metallic glasses, J. Alloy. Comp. 737 (2018) 815–820.
[20] J.S. Blazquez, C.F. Conde, A. Conde, Kinetics of nanocrystallization in FeCoNbB(Cu) alloys, Appl. Phys. A 76 (4) (2003) 571–575.
[21] Y. Wu, H.X. Li, J.E. Gao, H. Wang, X.J. Liu, M.K. Miller, H. Bei, Y.F. Gao, Z.P. Lu, Nanocrystallization in a Cu-doped Fe-based metallic glass, J. Alloy. Comp. 688 (2016) 822–827.
[22] T.C. Hufnagel, C.A. Schuh, M.L. Falk, Deformation of metallic glasses: recent developments in theory, simulations, and experiments, Acta Mater. 109 (2016) 375–393.
[23] S.G. Corcoran, R.J. Colton, E.T. Lilleodden, W.W. Gerberich, Anomalous plastic deformation at surfaces: nanoindentation of gold single crystals, Phys. Rev. B 55 (24) (1997) 16057–16060.
[24] A. Gouldstone, K.J. Van Vliet, S. Suresh, Nanoindentation - simulation of defect nucleation in a crystal, Nature 411 (6838) (2001), 656-656.
[25] A. Concustell, J. Sort, A.L. Greer, M.D. Baro, Anelastic deformation of a $Pd_{40}Cu_{30}Ni_{10}P_{20}$ bulk metallic glass during nanoindentation, Appl. Phys. Lett. 88 (17) (2006) 171911.
[26] B. Wei, T. Zhang, W. Li, D. Xing, L. Zhang, Y. Wang, Indentation creep behavior in Ce-based bulk metallic glasses, Mater. Trans. 46 (12) (2005) 2959–2962.
[27] W.H. Li, K. Shin, C.G. Lee, B.C. Wei, T.H. Zhang, Y.Z. He, The characterization of creep and time-dependent properties of bulk metallic glasses using nano-indentation, Mater. Sci. Eng. A 478 (1–2) (2008) 371–375.
[28] H. Li, A.H.W. Ngan, Size effects of nanoindentation creep, J. Mater. Res. 19 (2) (2004) 513–522.
[29] B.N. Lucas, W.C. Oliver, Indentation power-law creep of high-purity indium, Metall. Mater. Trans. A 30 (3) (1999) 601–610.
[30] W.B. Li, J.L. Henshall, R.M. Hooper, K.E. Easterling, The mechanisms of indentation creep, Acta Mater. 39 (12) (1991) 3099–3110.
[31] B. Storakers, P.L. Larsson, On Brignell and Boussinesq indentation of creeping solids, J. Mech. Phys. Solids 42 (2) (1994) 307–332.
[32] M. Heggen, F. Spaepen, M. Feuerbacher, Creation and annihilation of free volume during homogeneous flow of a metallic glass, J. Appl. Phys. 97 (3) (2005).
[33] F. Spaepen, Microscopic mechanism for steady-state inhomogeneous flow in metallic glasses, Acta Metall. 25 (4) (1977) 407–415.
[34] J.G. Wang, D.Q. Zhao, M.X. Pan, W.H. Wang, S.X. Song, T.G. Nieh, Correlation between onset of yielding and free volume in metallic glasses, Scr. Mater. 62 (7) (2010) 477–480.
[35] P. De Hey, J. Sietsma, A. Van den Beukel, Structural disordering in amorphous $Pd_{40}Ni_{40}P_{20}$ induced by high temperature deformation, Acta Mater. 46 (16) (1998) 5873–5882.
[36] M.J. Mayo, W.D. Nix, A micro-indentation study of superplasticity in Pb, Sn, and Sn-38 wt-percent-Pb, Acta Metall. 36 (8) (1988) 2183–2192.
[37] P.M. Sargent, M.F. Ashby, Indentation creep, Mater. Sci. Technol. 8 (7) (1992) 594–601.
[38] W.H. Poisl, W.C. Oliver, B.D. Fabes, The relationship between indentation and uniaxial creep in amorphous selenium, J. Mater. Res. 10 (8) (1995) 2024–2032.
[39] C.A. Schuh, T.G. Nieh, A nanoindentation study of serrated flow in bulk metallic glasses, Acta Mater. 51 (1) (2003) 87–99.
[40] C.C. Yuan, Z.W. Lv, C.M. Pang, X.L. Wu, S. Lan, C.Y. Lu, L.G. Wang, H.B. Yu, J.H. Luan, W.W. Zhu, G.L. Zhang, Q. Liu, Xun-Li Wang, B.L. Shen, Atomic-scale heterogeneity in large-plasticity Cu-doped metallic glasses, J. Alloy. Comp. 798 (2019) 517–522.
[41] J.J. Kim, Y. Choi, S. Suresh, A.S. Argon, Nanocrystallization during nano-indentation of a bulk amorphous metal alloy at room temperature, Science 295 (5555) (2002) 654–657.
[42] J.J. Lewandowski, W.H. Wang, A.L. Greer, Intrinsic plasticity or brittleness of metallic glasses, Philos. Mag. Lett. 85 (2) (2005) 77–87.
[43] A. Slipenyuk, J. Eckert, Correlation between enthalpy change and free volume reduction during structural relaxation of $Zr_{55}Cu_{30}Al_{10}Ni_5$ metallic glass, Scr. Mater. 50 (1) (2004) 39–44.
[44] A. Vandenbeukel, J. Sietsma, The glass-transition as a free-volume related kinetic phenomenon, Acta Metall. Mater. 38 (3) (1990) 383–389.
[45] C.C. Yuan, J. Ma, X.K. Xi, Understanding the correlation of plastic zone size with characteristic dimple pattern length scale on the fracture surface of a bulk metallic glass, Mater. Sci. Eng. A-Struct. Mater. Prop. Microstruct. Process. 532 (2012) 430–434.
[46] W.H. Li, B.C. Wei, T.H. Zhang, D.M. Xing, L.C. Zhang, Y.R. Wang, Study of serrated flow and plastic deformation in metallic glasses through instrumented indentation, Intermetallics 15 (5–6) (2007) 706–710.
[47] L. Liu, K.C. Chan, Plastic deformation of Zr-based bulk metallic glasses under nanoindentation, Mater. Lett. 59 (24–25) (2005) 3090–3094.
[48] J.T. Kim, S.H. Hong, C.H. Lee, J.M. Park, T.W. Kim, W.H. Lee, H.I. Yim, K.B. Kim, Plastic deformation behavior of Fe-Co-B-Si-Nb-Cr bulk metallic glasses under nanoindentation, J. Alloy. Comp. 587 (2014) 415–419.
[49] A.S. Argon, Plastic-deformation in metallic glasses, Acta Metall. 27 (1) (1979) 47–58.
[50] M.W. Chen, Mechanical behavior of metallic glasses: microscopic understanding of strength and ductility, Annu. Rev. Mater. Res. 38 (2008) 445–469.
[51] X.H. Du, J.C. Huang, K.C. Hsieh, Y.H. Lai, H.M. Chen, J.S.C. Jang, P.K. Liaw, Two-glassy-phase bulk metallic glass with remarkable plasticity, Appl. Phys. Lett. 91 (13) (2007) 131901.
[52] H. Gleiter, Nanoglasses: a new kind of noncrystalline material and the way to an age of new technologies? Small 12 (16) (2016) 2225–2233.
[53] G. Wu, K.-C. Chan, L. Zhu, L. Sun, J. Lu, Dual-phase nanostructuring as a route to high-strength magnesium alloys, Nature 545 (7652) (2017), 80-+.
[54] Y. Yang, J.F. Zeng, A. Volland, J.J. Blandin, S. Gravier, C.T. Liu, Fractal growth of the dense-packing phase in annealed metallic glass imaged by high-resolution atomic force microscopy, Acta Mater. 60 (2012) 5260–5272.
[55] J. Ding, S. Patinet, M.L. Falk, Y. Cheng, E. Ma, Soft spots and their structural signature in a metallic glass, Proc. Natl. Acad. Sci. 111 (2014) 14052–14056.
[56] P. Tsai, K. Kranjc, K.M. Flores, Hierarchical heterogeneity and an elastic microstructure observed in a metallic glass alloy, Acta Mater. 139 (2017) 11–20.
[57] B. Sarac, Y.P. Ivanov, A. Chuvilin, T. Schoberl, M. Stoica, Z.L. Zhang, J. Eckert, Origin of large plasticity and multiscale effects in iron-based metallic glasses, Nat. Commun. 9 (2018) 1333.
[58] T. Ichitsubo, E. Matsubara, T. Yamamoto, H.S. Chen, N. Nishiyama, J. Saida, K. Anazawa, Microstructure of fragile metallic glasses inferred from ultrasound-accelerated crystallization in Pd-based metallic glasses, Phys. Rev. Lett. 95 (24) (2005) 245501.
[59] D.B. Miracle, T. Egami, K.M. Flores, K.F. Kelton, Structural aspects of metallic glasses, MRS Bull. 32 (8) (2007) 629–634.